Calculation of Synchronous Reactances of Small Permanent-Magnet Alternating-Current Motors: Comparison of Analytical Approach and Finite Element Method with Measurements

Jacek F. Gieras, Ezio Santini, and Mitchell Wing

***Abstract*— The synchronous reactances of permanent magnet (PM) motors have been determined using: 1) analytical method, i.e., form factors of the stator field (armature reaction factors), 2) finite element method (FEM), and 3) experimental tests on a special machine set. The analytical method is widely used in calculations of synchronous reactances of salient pole synchronous machines with electromagnetic excitation. Rotors of PM synchronous machines have more complicated structures, hence it is more difficult to predict accurately the magnetic field distribution in their airgaps in order to find the form factors of the stator field. Numerical methods of field analysis can easily solve this problem. The FEM can predict both the synchronous and mutual (armature reaction) reactances in the d and q axes. The leakage reactance can then be evaluated as a difference between synchronous and mutual reactances. As an example, a small, three-phase, four-pole motor with SmCo surface mounted PM's (three parallel magnets per pole), and mild-steel pole shoes has been investigated. Such a complicated rotor structure has been intentionally designed in order to be able to compare the advantages and disadvantages of the analytical method and the FEM. In the FEM, the reactances have been calculated using both the *flux linkage* and *current/energy perturbation* method. Synchronous reactances as functions of the stator current and load angle obtained analytically from the FEM modeling and from measurements have been compared.**

***Index Terms*—Analytical approach, FEM, measurements, permanent magnet ac motors, synchronous reactance.**

I. Introduction

THE accuracy of calculating the steady-state performance of small permanent magnet (PM) synchronous motors depends on the accuracy of calculating the synchronous reactances in the d and q axes. For typical medium power and large synchronous motors with electromagnetic excitation analytical methods using *form factors of the stator (armature) magnetic flux density* are good enough. Small PM synchronous motors sometimes have a complicated structure, and numerical or analog modeling is necessary to obtain an accurate distribution of the magnetic field. This distribution is very helpful to correctly estimate the form factors of the rotor and stator magnetic flux densities.

The finite element method (FEM) makes it possible to find the d- and q-axis synchronous reactances and mutual (armature reaction) reactances by computing the corresponding inductances, e.g., [3], [4], [6], [18]–[20]. It can be done by using the flux linkage and magnetic vector potential concept or energy stored in the winding. Recently, two modern FEM techniques in ac machines analysis have emerged: *current/energy perturbation method* [7], [8], [15], [23] and *time-stepping analysis* [1], [5]. These methods are especially suitable for transient analysis of converter-fed PM synchronous machines.

The measurement of the synchronous reactances for small PM synchronous motors seems to be more difficult. There are several methods for the measurement of synchronous reactances of medium and large synchronous machines but the assumptions made do not allow one to apply these methods to small PM synchronous motors. In this paper a special laboratory setup is presented for the load angle δ estimation of small synchronous motors. The measured load angle, input voltage, armature current, armature winding resistance, and power factor allow for finding the synchronous reactances X_{sd} and X_{sq} on the basis of the phasor diagram.

II. Analytical Approach

As it is known the d- and q-axis synchronous reactances are defined as

$$X_{sd} = X_{ad} + X_1 \quad X_{sq} = X_{aq} + X_1 \tag{1}$$

where X_{ad} is the d-axis mutual (armature reaction) reactance, X_{aq} is the q-axis mutual reactance, and X_1 is the armature winding leakage reactance per phase. The reactance X_{ad} and sometimes X_{aq} depend on the magnetic saturation due to the main flux. The leakage reactance X_1 consists of the slot, differential, tooth–top, and end-connection leakage reactances. Only the slot and differential leakage reactances depend on the magnetic saturation due to leakage fields. It can be taken into account using Norman's method [16].

The analytical approach to calculating the synchronous reactances is based on the distribution of the stator winding normal component magnetic flux density. This distribution

Manuscript received March 31, 1996; revised March 12, 1998. This work was supported by the Foundation for Research Development (FRD) of the Republic of South Africa, Italian Ministry of Scientific and Technological Research, and the University of Rome, La Sapienza.

J. F. Gieras and M. Wing are with the Department of Electrical Engineering, University of Cape Town, Rondebosch 7700, South Africa (e-mail: gierasjf@utrc.utc.com).

E. Santini is with the Department of Electrical Engineering, University of Rome, La Sapienza, 00184 Rome, Italy.

Publisher Item Identifier S 0018-9464(98)06332-8.

can be assumed to be a periodic function of the stator inner perimeter or can be found using numerical or analog modeling.

The d-axis mutual reactance and q-axis mutual reactance are expressed in terms of *form factors* of the stator field (armature reaction factors) k_{fd} and k_{fq}, i.e., [12]

$$X_{ad} = k_{fd} X_a \quad X_{aq} = k_{fq} X_a. \tag{2}$$

The mutual reactance X_a is the same as that for a cylindrical-rotor synchronous machine

$$X_a = 4 m_1 \mu_0 f \frac{(N_1 k_{w1})^2}{\pi p} \frac{\tau L_i}{k_C g} \tag{3}$$

where m_1 is the number of stator (armature) phases, μ_0 is the permeability of free space, f is the input frequency, N_1 is the number of stator turns per phase, k_{w1} is the stator winding factor for the fundamental space harmonic, p is the number of pole pairs, τ is the pole pitch, L_i is the effective length of the armature core, k_C is Carter's coefficient for the airgap, and g is the airgap in the d-axis. To obtain a saturated synchronous reactance, the equivalent airgap $k_C g$ should be multiplied by the saturation factor $k_{\text{sat}} > 1$ of the magnetic circuit, i.e., to obtain $k_C k_{\text{sat}} g$. In most salient pole synchronous machines with electromagnetic excitation, the magnetic saturation affects only X_{sd} since the q-axis airgap is comparatively very large. In some PM synchronous machines the magnetic saturation affects both X_{sd} and X_{sq}.

The form factors of the stator field are defined as the ratios of the first harmonic amplitudes-to-the maximum values of normal components of stator (armature) magnetic flux densities in the d-axis and q-axis, respectively, i.e.,

$$k_{fd} = \frac{B_{ad1}}{B_{ad}} \quad k_{fq} = \frac{B_{aq1}}{B_{aq}}. \tag{4}$$

The peak values of the fundamental harmonics B_{ad1} and B_{aq1} of the stator magnetic flux density can be calculated as coefficients of Fourier series for the fundamental harmonic, i.e.,

$$B_{ad1} = \frac{4}{\pi} \int_0^{0.5\pi} B(x) \cos x \, dx$$
$$B_{aq1} = \frac{4}{\pi} \int_0^{0.5\pi} B(x) \sin x \, dx. \tag{5}$$

For the distributions of d- and q-axis, magnetic flux densities according to Fig. 1, the first harmonics of the magnetic flux densities are

i) in the case of inset-type PM's [Fig. 1(a)]

$$B_{ad1} = \frac{4}{\pi} \left[\int_0^{0.5\alpha\pi} (B_{ad} \cos x) \cos x \, dx + \int_{0.5\alpha\pi}^{0.5\pi} (c_g B_{ad} \cos x) \cos x \, dx \right]$$
$$= \frac{1}{\pi} B_{ad} [(\alpha\pi + \sin \alpha\pi) + c_g (\pi - \alpha\pi - \sin \alpha\pi)] \tag{6}$$

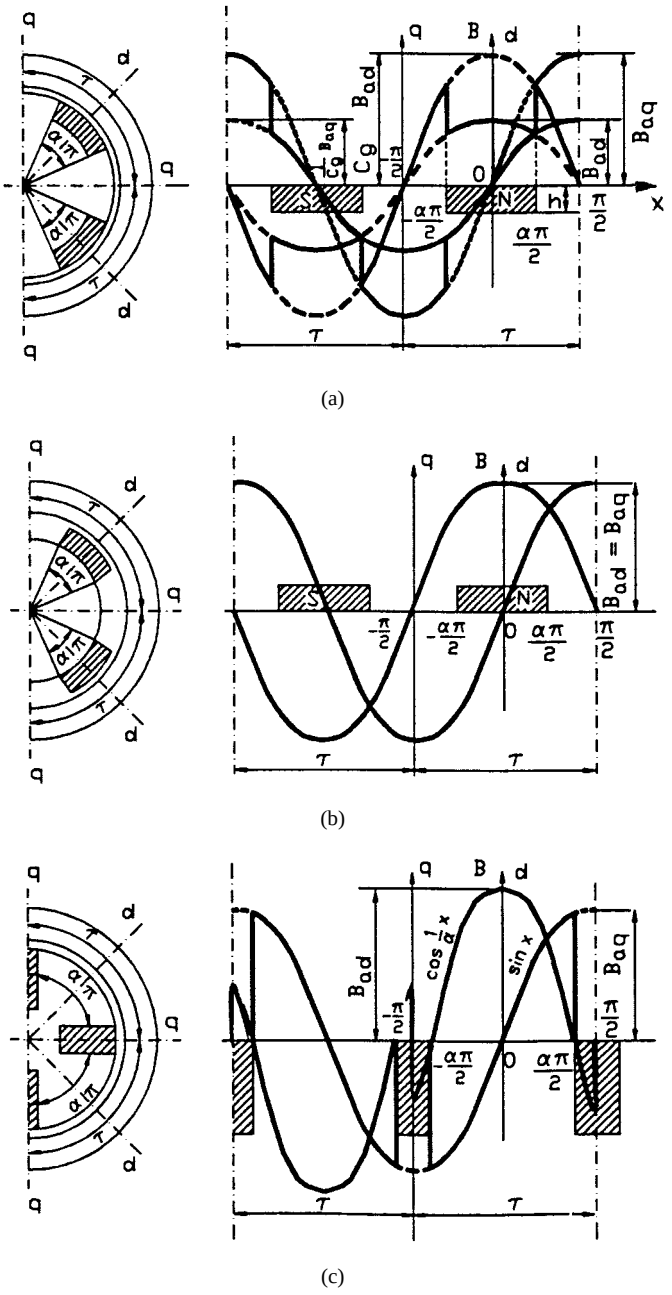

(a)

(b)

(c)

Fig. 1. Distribution of the d-axis and q-axis magnetic flux density for rare-earth PM rotors: (a) inset-type PM rotor, (b) surface PM's, and (c) buried PM rotor.

$$B_{aq1} = \frac{4}{\pi} \left[\int_0^{0.5\alpha\pi} \frac{1}{c_g} (B_{aq} \sin x) \sin x \, dx + \int_{0.5\alpha\pi}^{0.5\pi} (B_{aq} \sin x) \sin x \, dx \right]$$
$$= \frac{1}{\pi} B_{aq} \left[\frac{1}{c_g} (\alpha\pi - \sin \alpha\pi) + \pi - \alpha\pi + \sin \alpha\pi \right] \tag{7}$$

ii) in the case of surface PM's [Fig. 1(b)]

$$B_{ad1} = \frac{4}{\pi} \int_0^{0.5\pi} (B_{ad} \cos x) \cos x \, dx = B_{ad} \tag{8}$$

$$B_{aq1} = \frac{4}{\pi} \int_0^{0.5\pi} (B_{ad} \sin x) \sin x \, dx = B_{aq} \tag{9}$$

TABLE I
REACTION FACTORS FOR PM SYNCHRONOUS MACHINES

Rotor configuration	Coefficients k_{fd} and k_{fq}
Inset type PM rotor	$k_{fd} = \frac{1}{\pi}[\alpha\pi + \sin\alpha\pi + c_g(\pi - \alpha\pi - \sin\alpha\pi)]$ $k_{fq} = \frac{1}{\pi}[\frac{1}{c_g}(\alpha\pi - \sin\alpha\pi) + \pi - \alpha\pi + sin\alpha\pi]$
Surface PM rotor	$k_{fd} = k_{fq} = 1$
Buried PMs	$k_{fd} = \frac{4}{\pi}\alpha\frac{1}{1-\alpha^2}\sin\left[(1+\alpha)\frac{\pi}{2}\right]$ $k_{fq} = \frac{1}{\pi}(\alpha\pi - \sin\alpha\pi)$
Salient pole synchronous motor with field excitation winding	$k_{fd} = \frac{1}{\pi}(\alpha\pi + \sin\alpha\pi)$ $k_{fq} = \frac{1}{\pi}(\alpha\pi - \sin\alpha\pi)$

iii) in the case of buried PM's [Fig. 1(c)]

$$B_{ad1} = \frac{4}{\pi}B_{ad}\int_0^{0.5\alpha\pi}\cos\left(\frac{1}{\alpha}x\right)\cos x\,dx$$
$$= \frac{2}{\pi}B_{ad}\left[\frac{\alpha\sin(1+\alpha)x/\alpha}{1+\alpha} + \frac{\alpha\sin(1-\alpha)x/\alpha}{1-\alpha}\right]_0^{0.5\alpha\pi}$$
$$= \frac{4}{\pi}B_{ad}\alpha\frac{1}{1-\alpha^2}\sin\left[(1+\alpha)\frac{\pi}{2}\right] \quad (10)$$

$$B_{aq1} = \frac{4}{\pi}\int_0^{0.5\alpha\pi}(B_{aq}\sin x)\sin x\,dx$$
$$= \frac{2}{\pi}B_{aq}\int_0^{0.5\alpha\pi}(1-\cos x)\,dx$$
$$= \frac{1}{\pi}B_{aq}[\alpha\pi - \sin\alpha\pi]. \quad (11)$$

For inset type PM's the coefficient c_g expresses an increase in the d-axis armature magnetic flux density due to a decrease in the airgap [Fig. 1(a)] from $g+h$ to g where h is the depth of the slot for the PM. Since the magnetic voltage drop across $g+h$ is equal to the sum of the magnetic voltage drops across the airgap g and ferromagnetic tooth height h, the following equality can be written: $B_{ad}c_g g/\mu_0 + B_{Fe}h/(\mu_0\mu_r) = B_{ad}(g+h)/\mu_0$. Because $B_{Fe}h/(\mu_0\mu_r) \ll B_{ad}(g+h)/\mu_0$, the coefficient of increase in the magnetic flux density due to a decrease in the airgap is $c_g \approx 1 + h/g$. Of course, when $h = 0$, then $B_{ad1} = B_{ad}$, $B_{aq1} = B_{aq}$, and $k_{fd} = k_{fq} = 1$. It means that the machine behaves as a cylindrical rotor machine. Similarly, for the surface magnet rotor $k_{fd} = k_{fq} = 1$ [Fig. 1(b)], since the relative magnetic permeability of rare-earth PM's $\mu_r \approx 1$. For the buried magnet rotor the d-axis armature flux density changes as $\cos(x/\alpha)$ and the q axis armature flux density changes as $\sin x$ [Fig. 1(c)]. The parameter $\alpha = b_p/\tau$ is the ratio of the PM or pole shoe width b_p to the pole pitch τ and can also be expressed as an angle.

The coefficients k_{fd} and k_{fq} for different rotor configurations are given in Table I. The last row shows k_{fd} and k_{fq} for salient pole synchronous motors with electromagnetic excitation [12].

III. FEM

A. Approach

The two following concepts are the most frequently used in the FEM computations of the steady-state inductances:

1) the number of flux linkages of the coil, divided by the current in the coil;
2) the energy stored in the coil, divided by one-half the current squared.

Both concepts give identical results for linear inductances but not the same for nonlinear inductances [13].

If the incorrect potential distribution does not differ very greatly from the correct one, the error in energy is much smaller than that in potential [21]. Therefore, the steady-state inductances are often very accurately approximated even if the potential solution contains substantial errors.

In order to predict accurately the dynamic behavior and performance of a converter-fed PM brushless motor, one must have accurate knowledge of values of the self- and mutual winding dynamic inductance $d\Psi/di$ rather then the steady-state value Ψ/I [15].

In the early 1980's, the *current/energy perturbation method* of calculating inductances was proposed [7], [8], [15], [23]. This method is based upon consideration of the total energy stored in the magnetic field of a given device comprising n windings.

In the papers [8], [15] the self and mutual inductance terms of the various n windings have been expressed as the partial derivatives of the global stored energy w with respect to various winding current perturbations Δi_j. These derivatives can, be expanded around a "quiescent" magnetic field solution obtained for a given set of winding currents, in terms of various current perturbations $\pm\Delta i_j$ and $\pm\Delta i_k$ in the jth and kth windings and the resulting change in the global energy.

The details are given in [7], [8], [15], and [23]. For the two-dimensional (2-D) field distribution the current/energy perturbation method does not take into account the end winding leakage.

For the steady-state conditions a similar accuracy can be obtained calculating first the synchronous reactance, then mutual reactance, and finally the slot and differential leakage reactance as a difference between synchronous and mutual reactances.

In this paper the inductances will be found on the basis of *flux linkage, Stokes' theorem, and magnetic vector potential*, i.e.,

$$L = \frac{\Psi}{I} = \frac{\int_S \nabla\times\boldsymbol{A}\cdot d\boldsymbol{S}}{I} = \frac{\oint\boldsymbol{A}\cdot d\boldsymbol{l}}{I} \quad (12)$$

where $\boldsymbol{A}$ is the magnetic vector potential around the contour $\boldsymbol{l}$. The synchronous reactance is when the total flux (Ψ_{sd} or Ψ_{sq}) includes both mutual and leakage fluxes, i.e., the stator slot, tooth top, and differential leakage flux.

The magnetic flux through the airgap does not include the stator leakage, but simply the d-axis and q-axis linkage flux Ψ_{ad} or Ψ_{aq}. The first harmonics of these main fluxes give the mutual (magnetizing) reactances [19], [20]. A combination of the total fluxes Ψ_{sd}, Ψ_{sq}, and linkage fluxes Ψ_{ad} and Ψ_{aq} will give the stator leakage reactance (excluding the end connection leakage reactance).

If the armature current $I_a = 0$, then it follows that the normal component of the rotor magnetic flux density determines the location of the d-axis. A line integral through the airgap gives the distribution of the magnetic vector potential. The values of constant vector potential represent flux lines. Numerical Fourier analysis of this vector potential yields an analytical expression for the fundamental harmonic, i.e.,

$$A_z(p\alpha) = a_1 \cos(p\alpha) + b_1 \sin(p\alpha) = A_{01} \sin(p\alpha + \alpha_d) \quad (13)$$

where $A_{01} = \sqrt{a_1^2 + b_1^2}$ and $\alpha_d = \arctan(b_1/a_1)$. The angle α_d relates to the d-axis which is the y-axis of the FEM model since it shows the angle of zero crossing of the magnetic vector potential through the airgap line contour. This angle is usually found to be zero due to the symmetry in the machine. The q-axis is related to the d-axis by a shift of $\pi/(2p)$ thus $\alpha_q = \alpha_d + \pi/(2p)$.

B. Synchronous Reactances

In a 2-D FEM model the d-axis and q-axis synchronous reactances, respectively, excluding the end leakage flux are

$$X_{sd} = 2\pi f \frac{\Psi_{sd}}{I_{ad}} \quad X_{sq} = 2\pi f \frac{\Psi_{sq}}{I_{aq}} \quad (14)$$

where Ψ_{sd} and Ψ_{sq} are the magnitudes of the total fluxes in the d and q-axis, respectively, I_{ad} and I_{aq} are the magnitudes of the d-axis and q-axis stator currents, respectively, and f is the input frequency. The d-axis and q-axis fluxes are obtained from the combination of the phase belt linkages [3], [4], [6], [18]. According to the phasor diagram for a synchronous motor, the rotor excitation flux and d-axis armature flux are in the same direction while the q-axis armature flux is perpendicular.

The calculation of the synchronous reactances using (14) are sensitive to the values of I_{ad} and I_{aq}, respectively. This is due to the fact that in the full-load analysis of a PM synchronous motor the values of I_{ad} and I_{aq} both approach zero at different load angles. The rounding off errors that occur in the FEM, amplify the error in the synchronous reactance as the armature current components tend toward zero. The use of a constant current disturbance, in both I_{ad} and I_{aq}, solves this problem. The synchronous reactances are then

$$X'_{sd} = 2\pi f \frac{\Delta\Psi_{sd}}{\Delta I_{ad}} \quad X'_{sq} = 2\pi f \frac{\Delta\Psi_{sq}}{\Delta I_{aq}} \quad (15)$$

where $\Delta\Psi_{sd}$ and $\Delta\Psi_{sq}$ are the changes in flux linkages at the load point in the d-axis and q-axis, respectively, and ΔI_{ad} and ΔI_{aq} are the values of the d-axis and q-axis stator current disturbances, respectively.

The magnetic saturation that occurs in the loaded finite element solution should be transferred to the unloaded problem. This is done by storing the permeability of every element obtained from the loaded nonlinear magnetic field computation.

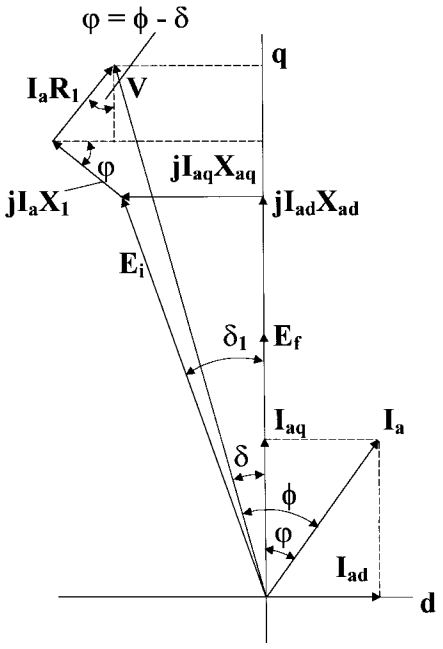

Fig. 2. Phasor diagram of a synchronous motor.

These permeabilities can then be used for the no-load linear calculation. This ensures that the saturation effect which occur in the loaded model is not ignored in the no-load results.

C. Mutual Reactances

The d-axis and q-axis fundamental components of magnetic flux in the airgap can be derived by performing a Fourier analysis on the vector potentials $\boldsymbol{A}$ around the inner surface of the armature core. In Fourier series the cosine term coefficient a_1 expresses the quantity of half the q-axis flux per pole and the sine term coefficient b_1 expresses the quantity of half the d-axis flux per pole [20]. Thus, the fundamental harmonic of the resultant flux per pole and the inner torque load angle δ_i (Fig. 2) are

$$\Phi = 2L_i \sqrt{a_1^2 + b_1^2} \quad \delta_i = \arctan\left(\frac{b_1}{a_1}\right). \quad (16)$$

This magnetic flux rotates at the synchronous speed $n_s = f/p$ (in revolutions per second) and induces in each phase winding the following internal EMF:

$$E_i = \pi\sqrt{2} f N_1 k_{w1} \Phi = \sqrt{(E_f \pm I_{ad} X_{ad})^2 + (I_{aq} X_{aq})^2}. \quad (17)$$

The phasor diagram shown in Fig. 2 gives the following expressions for the d-axis and q-axis mutual reactances:

$$X_{ad} = \frac{E_i \cos\delta_i - E_f}{I_{ad}} \quad (18)$$

$$X_{aq} = \frac{E_i \sin\delta_i}{I_{aq}}. \quad (19)$$

Armature reaction affects saturation of magnetic circuit at different loads. To take into account this effect another equation similar to (18) is used [20].

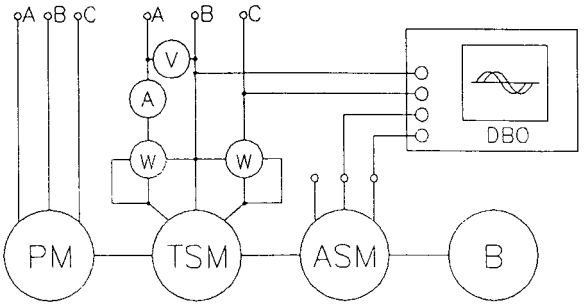

Fig. 3. Laboratory setup for measuring the load angle δ of PM synchronous motors: TSM — tested synchronous motor, ASM — additional synchronous motor with the same number of poles as TSM, PM — prime mover (synchronous or dc motor), B — brake, and DBO — dual-beam oscilloscope.

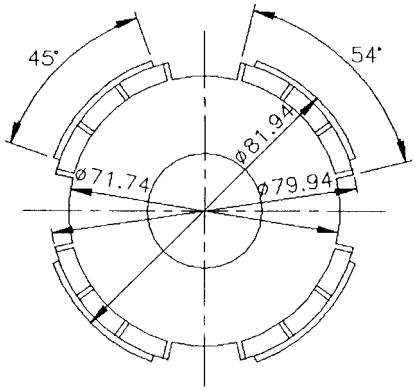

Fig. 4. Cross section of the tested PM rotor.

D. Leakage Reactance

The armature leakage reactance can be obtained in two ways:

1) from numerical evaluation of the energy stored in the slots and in the end connections;
2) as the difference between the synchronous reactance and armature reaction reactance, i.e.,

$$X_1 = X_{sd} - X_{ad} \quad \text{or} \quad X_1 = X_{sq} - X_{aq}. \tag{20}$$

In general, the calculation of the end connection leakage reactance is rather difficult using a 2-D FEM program and does not bring satisfactory results. For this purpose a three-dimensional FEM software is recommended [23].

IV. Experimental Method

A reliable method of measurement of synchronous reactances results from the phasor diagram (Fig. 2). Thus, the following equations can be written:

$$\begin{aligned} V\cos\delta &= E_f + I_{ad}X_{ad} + I_aX_1\sin(\phi-\delta) + I_aR_1\cos(\phi-\delta) \\ &= E_f + I_aX_{sd}\sin(\phi-\delta) + I_aR_1\cos(\phi-\delta) \end{aligned} \tag{21}$$

$$\begin{aligned} V\sin\delta &= I_aX_1\cos(\phi-\delta) + I_{aq}X_{aq} - I_aR_1\sin(\phi-\delta) \\ &= I_aX_{sq}\cos(\phi-\delta) - I_aR_1\sin(\phi-\delta). \end{aligned} \tag{22}$$

The d-axis synchronous reactance can be found from (21) and the q-axis synchronous reactance can be found from (22), i.e.,

$$X_{sd} = \frac{V\cos\delta - E_f - I_aR_1\cos(\phi-\delta)}{I_a\sin(\phi-\delta)} \tag{23}$$

$$X_{sq} = \frac{V\sin\delta + I_aR_1\sin(\phi-\delta)}{I_a\cos(\phi-\delta)}. \tag{24}$$

It is easy to measure the input voltage V, phase armature current I_a, armature winding resistance R_1 per phase, and the angle $\phi = \arccos[P_{in}/(m_1VI_a)]$. To measure the load angle δ it is recommended to use the equipment [17] as shown in Fig. 3. The EMF E_f induced by the rotor flux is assumed to be equal to the no-load EMF, i.e., at $I_a \approx 0$.

The terminals of the two corresponding phases of the tested synchronous motor (TSM) and additional synchronous motor (ASM) are connected to a dual-beam oscilloscope. The no-load EMF's $E_{f\mathrm{TSM}}$ of TSM and $E_{f\mathrm{ASM}}$ of ASM operating as generators should be in phase. Thus, the same positions of the TSM and ASM rotors with regard to the same phase windings can be found. When the TSM is connected to a three-phase power supply and the oscilloscope receives the signals V_{TSM} and $E_{f\mathrm{ASM}}$, the load angle δ can be measured, i.e., the phase angle between instantaneous values of V_{TSM} and $E_{f\mathrm{ASM}}$. Equations (23) and (24) allows for the investigation of how the input voltage V and load angle δ affect X_{sd} and X_{sq}. It is necessary to say that the accuracy of measurement of the angle δ much depends on the higher harmonic contents in V_{TSM} and $E_{f\mathrm{ASM}}$.

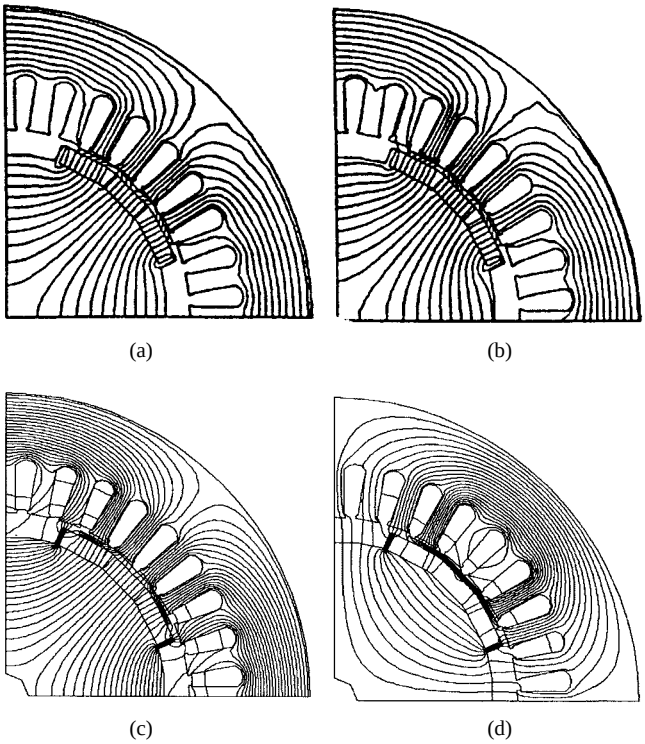

Fig. 5. Magnetic flux distribution (FEM) in the cross section of the tested motor: (a) at no-load, (b) with load at 10 Nm shaft torque, (c) d-axis stator flux, and (d) q-axis stator flux.

V. Experimental Verification of the Analytical Approach and FEM

A. Construction of the Tested Motor

The stator of a small 1.5-kW, 4-pole, 1410-rpm, 380-V, three-phase, Y-connected, cage induction motor manufactured

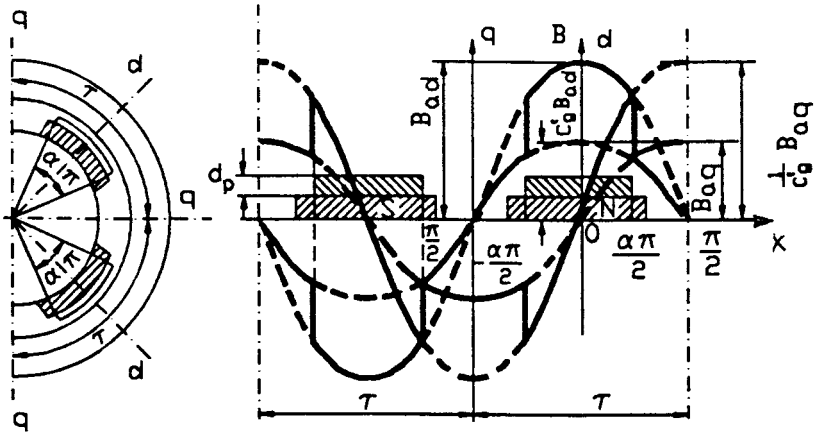

Fig. 6. Distributions of the d-axis and q-axis armature magnetic flux density in the airgap of the tested motor.

by GEC (South Africa) has been selected. The stator consists of a laminated core made of cold-rolled electrotechnical sheet-steel and a three-phase double-layer winding. There are 36 semi-open slots with the slot opening equal to 2.25 mm. The number of turns per phase is $N_1 = 240$ and the coil span is equal to the pole pitch. The stator inner diameter is 82.54 mm and the effective length of the armature stack is $L_i = 103$ mm.

The commercial cage rotor has been replaced with a surface PM rotor with mild-steel pole shoes [10]. The yoke and shaft have been made of one piece of a solid carbon steel. The length of the rotor solid core is 100 mm. Three parallel 10-mm wide and 5-mm thick surface SmCo PM's per pole have been designed as shown in Fig. 4. To reduce the airgap, make the motor self-starting, and improve its stability, the PM's have been equipped with thin mild-steel pole shoes covering 83% of the width of PM's. The d-axis airgap (mechanical clearance) is $g = 0.3$ mm, the q-axis airgap is $g_q = 5.4$ mm, and the thickness of the mild-steel pole shoe is $d_p = 1$ mm. The PM's have been magnetized radially.

Fig. 5 shows the magnetic flux distribution through the cross section of the motor as obtained with the aid of the FEM. The d-axis and q-axis magnetic flux density distributions in the airgap along the pole pitch are plotted in Fig. 6.

B. Analytical Approach

The form factors of the armature reaction can be derived on the basis of Fig. 6, similarly to those in Section II. For the surface PM rotor with mild-steel pole shoes the d and q-axis form factors are

$$k_{fd} = \frac{1}{\pi}[\alpha\pi + \sin\alpha\pi + c'_g(\pi - \alpha\pi - \sin\alpha\pi)] \quad (25)$$

$$k_{fq} = \frac{1}{\pi}\left[\frac{1}{c'_g}(\alpha\pi - \sin\alpha\pi) + \pi - \alpha\pi + \sin\alpha\pi\right]. \quad (26)$$

The coefficient $c'_g \approx 1 - d_p/g_q < 1$ is evaluated in a similar way as the coefficient c_g in Section II, where d_p is the thickness of the mild-steel pole shoe and g_q is the airgap in q axis. For the tested machine $c'_g = 0.8148$. The form factors k_{fd} and k_{fq} versus α for the rotor with surface PM's and mild-steel pole shoes are shown in Fig. 7. For the rotor of the tested motor $\alpha = b_p/\tau = 45^0/90^0 = 0.5$. Then the leakage reactance $X_1 = 2.014\,\Omega$ ($I_a = 0, k_C = 1.0258$) and armature reaction reactanes $X_{ad} = 9.102\ \Omega$ and $X_{aq} = 9.8082\ \Omega$ according to (2), (3), (25), and (26) have been calculated for $f = 50$ Hz. For $I_a = 7.5$ A the leakage reactance $X_1 = 1.677\ \Omega$. This reduction is caused by the magnetic saturation due to leakage fields [16]. In order to find the leakage reactances, classical equations for slot (double-layer winding), end-connection, differential, and tooth-top leakage permeances have been used [12].

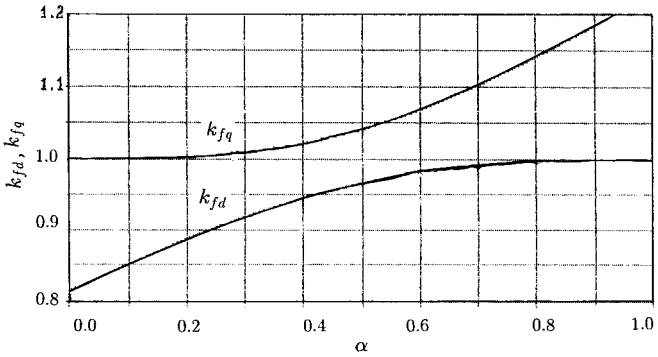

Fig. 7. Form factors k_{fd} and k_{fq} as functions of $\alpha = b_p/\tau$ for the surface PM rotor with thin mild-steel pole shoes.

However, X_{ad} and X_{aq} have been obtained with the magnetic saturation due to the main flux being neglected. Fig. 8 shows the mutual reactances X_{ad} and X_{aq} plotted against the armature current for the analytical approach ($k_{\rm sat} = 1$).

The synchronous reactances according to (1) at $f = 50$ Hz, $I_a = 0$, and $k_{\rm sat} = 1$ are $X_{sd} = 11.12\,\Omega$ and $X_{sq} = 11.82\,\Omega$.

C. FEM

The computation on the basis of the FEM shows that the mutual reactances are dependent on the armature current (Fig. 8) which means that the magnetic saturation is included. Owing to the thin mild-steel pole shoe which is subject to the magnetic saturation, the q-axis mutual reactance is more sensitive to the armature current than the d-axis reactance [see also Fig. 5(c) and (d)].

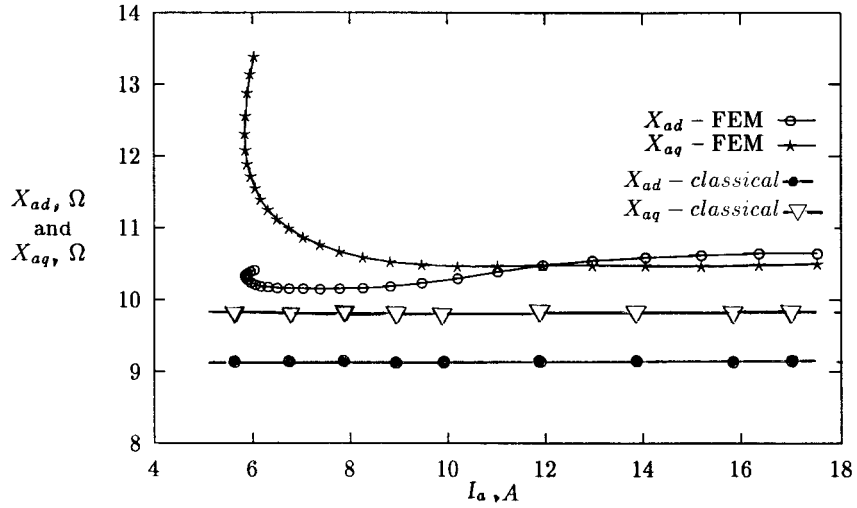

Fig. 8. X_{ad} and X_{aq} as functions of the *rms* stator current I_a at $f = 50$ Hz. Computation results using analytical approach and FEM.

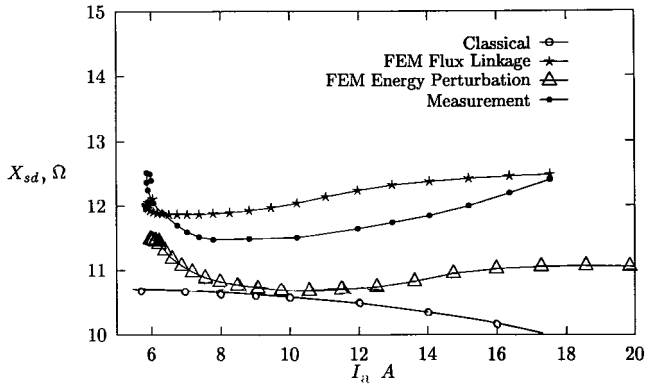

(a)

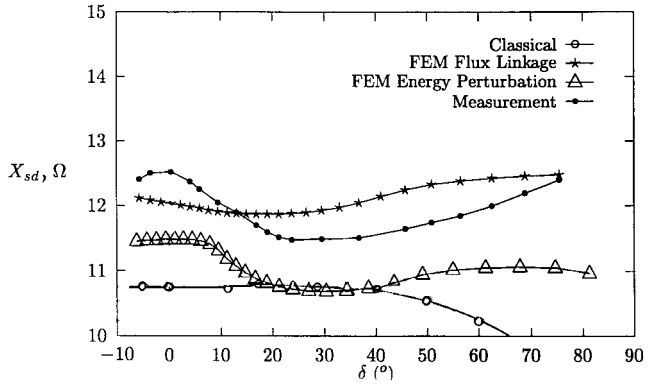

(b)

Fig. 9. Synchronous reactance X_{sd} at constant terminal voltage of 220 V and $f = 50$ Hz versus: (a) the stator current I_a and (b) the load angle δ.

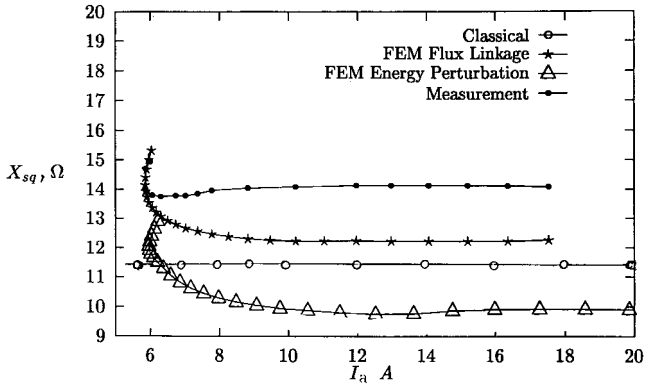

(a)

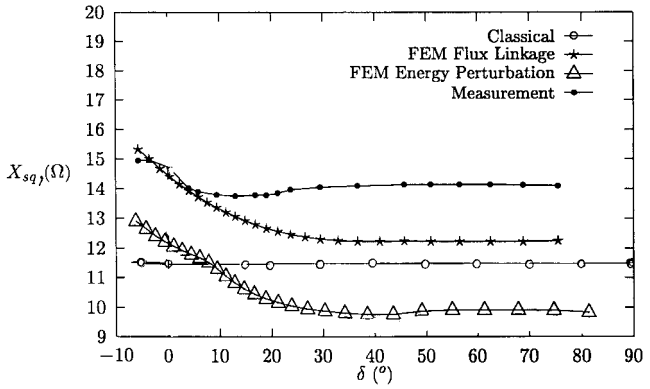

(b)

Fig. 10. Synchronous reactances X_{sq} at constant terminal voltage of 220 V and $f = 50$ Hz versus: (a) the stator current I_a and (b) the load angle δ.

The calculation of the leakage reactances has been done using (20).

D. Experimental Tests

Experimental tests have been performed using the machine set according to Fig. 3. It was possible to test the motor only in the range of the stator current from 5.7–17.5 A. The no-load current is approximately 5.7 A.

E. Comparison

Figs. 9 and 10 show the d-axis and q-axis synchronous reactances obtained from analytical, finite element, and experimental methods. In both cases, the FEM results are closer to the test results than those obtained from the analytical approach.

The load angle δ in the range of armature current $5.7 \leq I_a \leq 17.5$ A can be both positive or negative. Consequently, the stator current I_a decreases and then increases as the angle

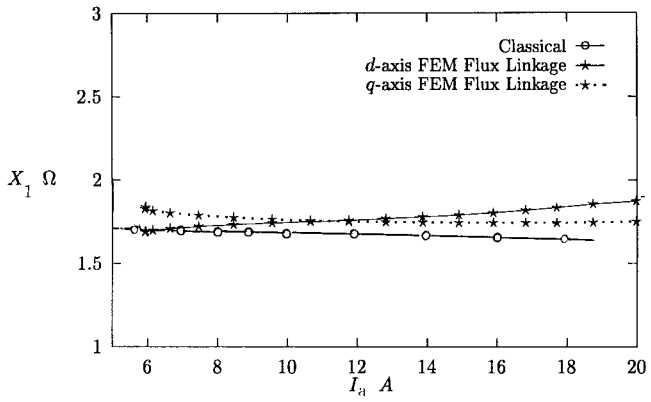

Fig. 11. Stator leakage reactance X_1 versus armature current I_a at $f = 50$ Hz.

between E_f and I_a increases from negative to positive values. This is why two values of X_{sd} and X_{sq} for small values of the armature current I_a have been obtained [Figs. 9(a) and 10(a)]. Classical approach neglects this effect.

The computation of the leakage reactance X_1 on the basis of the FEM gives slightly different results when using $X_{sd} - X_{ad}$ and $X_{sq} - X_{aq}$. Both results are very close to the analytical results (Fig. 11).

VI. Conclusion

The analytical and finite element approach to calculating the synchronous reactances have been compared with the experimental tests on a new type of PM synchronous motor with surface PM's and mild-steel pole shoes. A full comparative analysis (FEM flux linkage, FEM current/energy perturbation, classical approach, and measurements) of reactances for wide range of the load has been done.

Since the popularity of PM synchronous motors in modern electric drives has recently increased, there is a need for reliable methods of prediction of operating characteristics for newly designed machines. The accuracy of calculating the armature current, electromagnetic power, and electromagnetic torque of a synchronous motor depends first of all on the correct evaluation of the synchronous reactances X_{sd} and X_{sq}.

Although simple analytical equations describing the form factors of the armature field are adequate for evaluating the synchronous reactances of typical salient-pole synchronous machines with electromagnetic excitation, they cannot always bring good results in the case of small PM motors. PM ac motors often have intricate rotor structure and the airgap magnetic field is difficult to express by analytical equations. In the tested motor with surface PM's and thin mild-steel pole shoes, the FEM gives better results than the analytical approach (Figs. 9 and 10). Hence, the classical analytical approach is not recommended in designing high-performance PM synchronous machines for modern electric drive systems.

For experimental verification of synchronous reactances a combination of the equation resulting from the phasor diagram and measurement of the load angle δ on a multimachine set is recommended. In this way the difficult problem of laboratory measurements of X_{sd} and X_{sq} for small synchronous motors seems to be successfully solved.

References

[1] A. Arkkio, "Time stepping finite element analysis of induction motors," presented at *Int. Conf. Elect. Mach. ICEM'88*, Pisa, Italy, 1988, vol. 1, pp. 275–290.

[2] V. A. Balagurov, F. F. Galtieev, and A. N. Larionov, *Permanent Magnet Electrical Machines*, (in Russian). Moscow, Russia: Energia, 1964.

[3] M. V. K. Chari and P. P. Silvester, "Analysis of turboalternator magnetic fields by finite elements," *IEEE Trans. Power Appart. Syst.*, vol 92, pp. 454–464, 1973.

[4] M. V. K. Chari, Z. J. Csendes, S. H. Minnich, S. C. Tandon, and J. Berkery, "Load characteristics of synchronous generators by the finite-element method," *IEEE Trans. Power Appart. Syst.*, vol. 100, no. 1, pp. 1–13, 1981.

[5] A. Demenko, "Time stepping FE analysis of electric motor drives with semiconductor converters," *IEEE Trans. Magn.*, vol. 30, pp. 3264–3267, Sept. 1994.

[6] N. A. Demerdash and H. B. Hamilton, "A simplified approach to determination of saturated synchronous reactances of large turbogenerators under load," *IEEE Trans. Power Appart. Syst.*, vol. 95, no. 2, pp. 560–569, 1976.

[7] N. A. Demerdash, F. A. Fouad, and T. W. Nehl, "Determination of winding inductances in ferrite type permanent magnet electric machinery by finite elements," *IEEE Trans. Magn.*, vol. 18, pp. 1052–1954, Nov. 1982.

[8] N. A. Demerdash, T. M. Hijazi, and A. A. Arkadan, "Computation of winding inductances of permanent magnet brushless dc motors with damper windings by energy perturbation," *IEEE Trans. Energy Conversion*, vol. 3, no. 3, pp. 705–713, 1988.

[9] E. F. Fuchs and E. A. Erdélyi, "Determination of waterwheel alternator steady-state reactances from flux plots," *IEEE Trans. Power Appart. Syst.*, vol. 91, pp. 2510–2527, 1972.

[10] J. F. Gieras and M. Wing, *Permanent Magnet Motors Technology: Design and Applications*. New York: Marcel Deker, 1996.

[11] V. B. Honsinger, "Performance of polyphase permanent magnet machines," *IEEE Trans. Power Appart. Syst.*, vol. 99, no. 4, pp. 1510–1516, 1980.

[12] M. Kostenko and L. Piotrovsky, *Electrical Machines*, vol. 2. Moscow, Russia: Mir Publishers, 1974.

[13] D. A. Lowther and P. P Silvester, *Computer-Aided Design in Magnetics*. Berlin: Springer-Verlag, 1986.

[14] S. A. Nasar, I. Boldea, and L. E. Unnewehr, *Permanent Magnet, Reluctance, and Self-Synchronous Motors*. Boca Raton, FL: CRC Press, 1993.

[15] T. W. Nehl, F. A. Fouad, and N. A. Demerdash, "Determination of saturated values of rotating machinery incremental and apparent inductances by an energy perturbation method," *IEEE Trans. Power Appart. Syst.*, vol. 101, no. 12, pp. 4441–4451, 1982.

[16] H. M. Norman, "Induction motor locked saturation curves, *Elec. Eng.*, pp. 536–541, 1934.

[17] I. L. Osin, V. P. Kolesnikov, and F. M. Yuferov, *Permanent Magnet Synchronous Micromotors*, (in Russian). Moscow, Russia: Energia, 1976.

[18] D. Pavlik, V. K. Garg, J. R. Repp, and J. Weiss, "A finite element technique for calculating the magnet sizes and inductances of permanent magnet machines," *IEEE Trans. Energy Conversion*, vol. 3 no. 1, pp. 116–122, 1988.

[19] M. A. Rahman and A. M. Osheiba, "Performance of large line-start permanent magnet synchronous motors," *IEEE Trans. Energy Conversion*, vol. 5, no. 1, pp. 211–217, 1990.

[20] M. A. Rahman and P. Zhou, "Determination of saturated parameters of PM motors using loading magnetic fields," *IEEE Trans. Magn.*, vol. 27, pp. 3947–3950, Sept. 1991.

[21] P. P. Silvester and R. L. Ferrari, *Finite Elements for Electrical Engineers*, 2nd ed. Cambridge, U.K.: Cambridge Univ. Press, 1990.

[22] W. Szeląg, "Numerical method for determining the parameters of permanent magnet synchronous motors," presented at *12th Symp. Electromagn. Phenomena Nonlinear Circuits*, Poznan, Poland, 1991, pp. 331–335.

[23] R. Wang and N. A. Demerdash, "Comparison of load performance and other parameters of extra high speed modified Lundell alternators for 3-D-FE magnetic field solutions," *IEEE Trans. Energy Conversion*, vol. 7, no. 2, pp. 342–352, 1992.

Jacek F. Gieras graduated in 1971 from the Technical University of Lódź, Poland. He received the Ph.D. degree in 1975 and D.Sc. (Dr hab) degree in 1980 from the University of Technology, Poznań, Poland.

From 1971 to 1987, he was with Poznań University of Technology, Poznań, and Academy of Technology and Agriculture, Bydgoszcz, Poland. In 1975 and 1976, he was a Visiting Researcher at the Czechoslovak Academy of Sciences, Prague, Czechoslovakia. From 1983 to 1985, he was a Research Visiting Professor at Queen's University, Kingston, Ontario, Canada. In 1987, he was promoted in Poland to the rank of Full Professor (life title) in Electrical Engineering. From 1987 to 1989, he was with the Department of Electrical Engineering at Jordan University of Science and Technology, Irbid, the Hashemite Kingdom of Jordan. From 1989 to 1998, he was with the Department of Electrical Engineering at the University of Cape Town, South Africa. In 1994, he was a Visiting Professor at the University of Rome, La Sapienza, Italy. In 1996, he was a Japan Railway Central Company Visiting Professor (Endowed Chair in Transportation System Engineering) at the University of Tokyo, Japan. In 1996 and 1997, he was a Guest Professor at Chungbuk National University, Cheongju, South Korea. He is now involved in high technology research in the United States. He has authored and co-authored 6 books and about 200 papers and patents. The best known books are *Linear Induction Drives* (London, U.K.: Oxford Univ. Press, 1994) and *Permanent Magnet Motor Technology: Design and Applications* (New York: Marcel Deker, 1996) co-authored with Dr. M. Wing.

Mitchell Wing received the B.Sc. degree in 1990, M.Sc. degree in 1992, and Ph.D. degree in 1996 in electrical engineering from the University of Cape Town, South Africa.

Currently, he is a Postdoctoral Fellow in the Department of Electrical Engineering at the University of Cape Town. He co-authored about 30 papers on permanent magnet electrical machines and one book, *Permanent Magnet Motor Technology: Design and Applications* (New York: Marcel Deker, 1996).